

# Vehicle Velocity Observer Design Using 6-D IMU and Multiple-Observer Approach

Jiwon J. Oh and Seibum B. Choi, *Member, IEEE*

**Abstract**—This paper mainly focuses on the accurate estimation of the vehicle velocities of all axes, using the data received from a low-cost 6-D inertial measurement unit. The data include the vehicle linear acceleration and angular rates of all axes. In addition, the observer uses the wheel speed sensors and steering wheel angle information, which are already available on most recent production cars. Utilizing the aforementioned information, based on the combination of a bicycle model and a kinematic model, a multiple-observer system that computes the weighted sum estimation that is dependent on cornering stiffness adaptation is adopted to observe the lateral vehicle velocity, as well as longitudinal and vertical velocities. The stability of each component of the proposed observer is investigated, and a set of assessments to confirm the performance of the entire system is arranged through experiments using a real production sport utility vehicle.

**Index Terms**—Adaptive algorithm, observers, state estimation, vehicle dynamics.

## NOMENCLATURE

|            |   |
|------------|---|
| $m$        | Vehicle mass.                                 |
| $g$        | Gravitational constant.                       |
| $h$        | Height of the center of gravity (CG).         |
| $l_f$      | Distance between the CG and the front axle.   |
| $l_r$      | Distance between the CG and the rear axle.    |
| $L$        | Distance between the front and rear axles.    |
| $I_y$      | Moment of inertia about the $y$ -axis.        |
| $I_z$      | Moment of inertia about the $z$ -axis.        |
| $\alpha_f$ | Front-tire slip angle.                        |
| $\alpha_r$ | Rear-tire slip angle.                         |
| $C_f$      | Front-tire cornering stiffness.               |
| $C_r$      | Rear-tire cornering stiffness.                |
| $\delta_f$ | Front-tire steering angle.                    |
| $\beta$    | Side-slip angle at the CG.                    |
| $v_x$      | Longitudinal velocity at the CG.              |
| $v_y$      | Lateral velocity at the CG.                   |
| $v_z$      | Vertical velocity at the CG.                  |
| $a_x$      | Longitudinal acceleration measured at the CG. |

Manuscript received August 21, 2011; revised December 12, 2011, February 10, 2012 and April 19, 2012; accepted June 9, 2012. Date of publication July 10, 2012; date of current version November 27, 2012. This work was supported in part by Hyundai Motor Company through the government-supported R&D project Development of Integrated X-by-Wire System With Information Fusion of Surrounding and Vehicle Sensors and by the National Research Foundation of Korea through the Korean government [Ministry of Education Science and Technology] under Grant 2012-0000991. The Associate Editor for this paper was X. Zhang.

The authors are with the Department of Mechanical Engineering, Korea Advanced Institute of Science and Technology, Daejeon 305 701, Korea (e-mail: jwo@kaist.ac.kr; sbchoi@kaist.ac.kr).

Color versions of one or more of the figures in this paper are available online at <http://ieeexplore.ieee.org>.

Digital Object Identifier 10.1109/TITS.2012.2204984

|          |   |
|----------|---|
| $a_y$    | Lateral acceleration measured at the CG.  |
| $a_z$    | Vertical acceleration measured at the CG. |
| $\phi$   | Roll angle.                               |
| $\theta$ | Pitch angle.                              |
| $\psi$   | Yaw angle.                                |
| $p$      | Roll rate measured at the CG.             |
| $q$      | Pitch rate measured at the CG.            |
| $r$      | Yaw rate measured at the CG.              |
| $F_{yf}$ | Front axle lateral tire force.            |
| $F_{yr}$ | Rear axle lateral tire force.             |
| $F_{zf}$ | Front axle vertical tire force.           |
| $F_{zr}$ | Rear axle vertical tire force.            |

## I. INTRODUCTION

The technological advancement of the automobile and its proliferation not only brought a noteworthy convenience to its users through a significant reduction of transportation time but has given rise to serious safety issues as well. Efforts have continued to prevent the effect of the latter issue from outgrowing that of the former merit, and one of their forms has emerged as the development of the electronic vehicle safety assist technologies [1]–[3], such as the electronic stability program, crash-avoidance systems aided by active front steering, and continuous damping control (CDC). Such technologies undoubtedly magnify the importance of accurate real-time identification of the ground vehicle states, because the aforementioned vehicle safety and comfort systems require reliable vehicle state information, whose estimation is the ultimate objective of this paper. Knowledge of the vehicle states may also facilitate the practical applications of the existing positioning algorithms [4]–[7] through the addition of improved dead reckoning accuracy when the Global Positioning System (GPS) information is less reliable.

For this paper, a 6-D inertial measurement unit (IMU) of the most cost-effective price range is used. With regard to the development of a production vehicle, cost is a crucial factor that determines the consumer price of the final product. Hence, the cost for realizing various vehicle safety technologies must be minimized to make them affordable for the users. At the same time, the scope of this paper is to secure the estimation performance, which is as reliable as that with using high-cost sensors, regardless of the types and severity of vehicle motion. Another contribution of this paper is to prevent any loss of state estimation accuracy, which may have occurred by discarding the GPS feedback availability. Independence from GPS use is advantageous, because vehicle state estimation performance is maintained under the GPS outage condition, such as in urban

areas surrounded by high-rise buildings, underground levels, or tunnels. The need to satisfy every aspect of these criteria has served as the major difficulty in previous studies to design wholly satisfactory vehicle velocity estimation algorithms [8]–[20]. Taking some representative previous publications, Farrelly and Wellstead [10] suggested a linear time-varying observer based on the kinematic model. Although it showed robust estimation performance even under the conditions of nonlinear tire characteristics and vehicle model parameter uncertainties, its estimation is sensitive to sensor error. Kaminaga and Naito [12] suggested a Lyapunov-based adaptive observer, but the consideration of road angle disturbance was overlooked.

In general, a vehicle-model-based observer is known to provide accurate estimation performance that is insensitive to sensor error. However, its performance may fluctuate with the vehicle model parameter errors. On the other hand, a vehicle kinematic observer is known to show robust estimation performance under the effect of vehicle model parameter error but is, in fact, sensitive to the sensor error. Previous works attempted to use both models to compensate for the weakness of one another. Some of the works that fall into such a category are listed as follows.

Fukada [13] proposed the combination of the observer based on the linear tire model and the direct integration of the sensor kinematics, but the estimation performance was limited when the tire showed strongly nonlinear characteristic such as in the case of a J-turn. Lee [16] suggested a method of using a simple bicycle-model-based observer estimation result as a pseudomeasurement of a kinematic observer, but an unclear assumption was involved in obtaining the observer gain, and consideration of the effect of sensor error was overlooked.

This paper contributes to combine the strengths of the model-based observer as well as the kinematic observer. One novel distinction to be noted, however, is that the proposed model systematically divides the domain of observer feedback function into four different sections to adjust the weightings assigned for each type of observer model. Such a technique is henceforth referred to as the observer synthesis [21]. It enables the juxtaposition of multiple estimations, which raises the observer performance of the vehicle lateral velocity and, hence, of other vehicle states, under a wider range of driving conditions.

This paper is organized as follows. To facilitate the flow of logic, Section II-A first displays the general layout of the observer with the block diagram. Section II-B deals with the core contribution of this paper, i.e., observer synthesis procedure, which juxtaposes the reference lateral velocities obtained by multiple observers. Section II-C briefly deals with the principle behind the primary longitudinal velocity approximation based on the wheel angular velocities. Section II-D deals with the method of cornering stiffness adaptation. Section II-E focuses on the bicycle-model-based observer. Section II-F describes the pseudointegration process, which uses the 6-D IMU measurements. Section II-G deals with the principal kinematic observer, which finalizes the three-axis velocity estimation using the result of the observer synthesis. Section III displays the results of the real car-based experiments performed under various different scenarios, after giving a thorough description of the test environments.

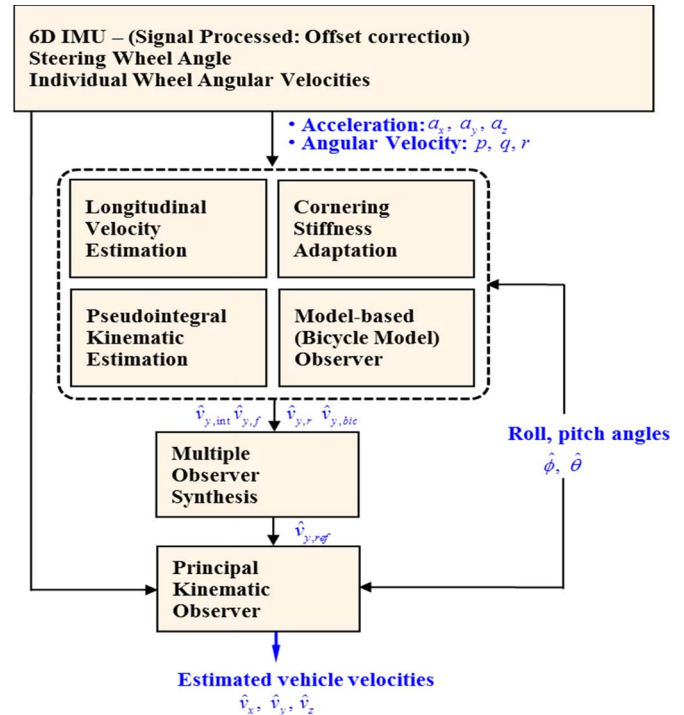


Fig. 1. General flow structure of the subcomponents of the suggested observer.

## II. OBSERVER DESIGN

### A. General Observer Flow Chart

The general structure of the entire observer is described in Fig. 1.

Making use of the available input signals from the sensors that are compensated by the externally observed vehicle roll and pitch angles [22], the vehicle lateral velocity at its center of gravity (CG) is estimated using four independent sources. The bicycle-model-based observer provides  $\hat{v}_{y,bic}$ , front and rear cornering stiffness estimation, each providing  $\hat{v}_{y,f}$  and  $\hat{v}_{y,r}$ , and the vehicle-kinematics-based pseudointegration provides  $\hat{v}_{y,int}$ . The synthesis of these interim estimations give  $\hat{v}_{y,ref}$ , the reference lateral velocity estimation used as the feedback term for the principal kinematic observer that simultaneously estimates the final longitudinal, lateral, and vertical vehicle velocities.

### B. Synthesis of Multiple Observers

The major contribution of this paper is the introduction of the observer synthesis and the methods of obtaining the four sources of lateral velocity, which generates an effective feedback reference for the principal kinematic observer, which will to be dealt with later. Here, the lateral velocity sources interact as a function of the front and rear cornering stiffness, which is obtained in Section II-E. The purpose of incorporating different sources is to make use of the bicycle model as much as possible so that the reference value that is finally obtained prevents the principal kinematic observer estimation from drifting away.

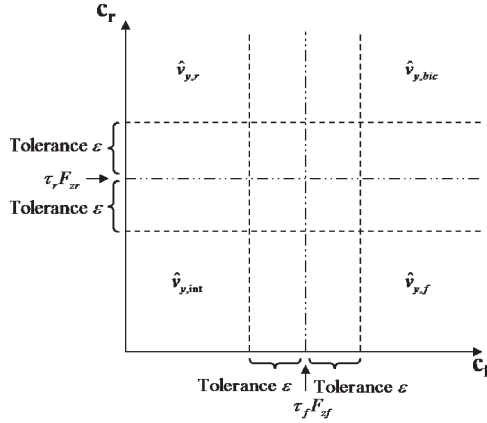


Fig. 2. Weighted sum estimation performed by the observer synthesis.

The calculation of this feedback  $\hat{v}_{y,ref}$  for the principal kinematic observer is based on selecting the appropriate lateral velocity among the following four sources:

- 1)  $\hat{v}_{y,bic}$ ;
- 2)  $\hat{v}_{y,f}$ ;
- 3)  $\hat{v}_{y,r}$ ;
- 4)  $\hat{v}_{y,int}$ .

The background principles on obtaining  $\hat{v}_{y,bic}$  and  $\hat{v}_{y,int}$  are dealt in Sections II-D and F, respectively, whereas the background principles on obtaining  $\hat{v}_{y,f}$  and  $\hat{v}_{y,r}$  are dealt with in Section II-E.

It is worthwhile here to state the rationale behind the effectiveness of implementing multiple observers on top of the cornering stiffness adaptation. Surely, if cornering stiffness adaptation alone sufficiently guarantees the accuracy of bicycle model, multiple observers are no longer necessary. However, although the use of the cornering stiffness adaptation technique improves the validity of the linear tire model, it is nearly impossible to take all disturbances that are not modeled either in the bicycle model or adaptation into consideration.

For example, unmodeled nonlinearity, which may be involved in the discrepancies among tire pressure or road friction coefficients, would cause the accuracy to significantly deteriorate. Thus, with regard to the nature of the linear bicycle model, it is certainly wise to make use of it in the linear region as much as possible, i.e., when the tire property majorly involves the linear characteristics. To realize this case, using the four pieces of lateral velocity information is the most appropriate if it is scheduled, as shown in Fig. 2.

Here,  $\varepsilon$  is a positive constant that denotes the tolerance range, and  $\tau_f$  and  $\tau_r$  are the positive constants that tune the threshold among the four sources as a function of the front and rear vertical loads.

As intended, the domain of the valid bicycle model use is maximized by emphasizing  $\hat{v}_{y,f}$  when  $C_f$  is high and emphasizing  $\hat{v}_{y,r}$  when  $C_r$  is high. As far as the typical tire characteristic with regard to the lateral force versus tire slip angle relationship, as shown in Fig. 3, is concerned, the cornering stiffness rapidly decreases beyond the linear region.

This case states that making use of the reference that corresponds to high cornering stiffness effectively avoids the nonlinearity.

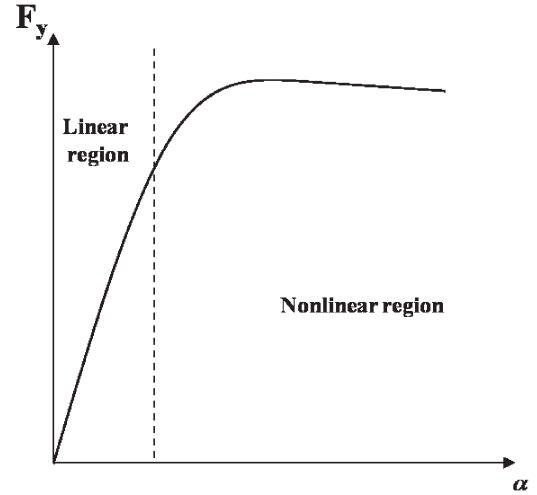


Fig. 3. Typical plot of tire lateral force versus slip angle.

For a smooth concoction of the lateral velocities, a sine function is taken to mix the sources in the tolerance region. According to the following equation,  $\hat{v}_{y,ref}$  is finally obtained by the observer synthesis:

$$\begin{aligned}
 \hat{v}_{y,ref} &= f(C_f, C_r, \hat{v}_{y,bic}, \hat{v}_{y,f}, \hat{v}_{y,r}, \hat{v}_{y,int}) \\
 &= \left[ \sin\left(\frac{\pi}{2\varepsilon}(C_f - \tau_f F_{zf})\right) \right. \\
 &\quad \times \left. \sin\left(\frac{\pi}{2\varepsilon}(C_r - \tau_r F_{zr})\right) \right] \hat{v}_{y,bic} \\
 &\quad + \left[ \sin\left(\frac{\pi}{2\varepsilon}(C_f - \tau_f F_{zf})\right) \right. \\
 &\quad \times \left. \left\{ 1 - \sin\left(\frac{\pi}{2\varepsilon}(C_r - \tau_r F_{zr})\right) \right\} \right] \hat{v}_{y,f} \\
 &\quad + \left[ \left\{ 1 - \sin\left(\frac{\pi}{2\varepsilon}(C_f - \tau_f F_{zf})\right) \right\} \right. \\
 &\quad \times \left. \sin\left(\frac{\pi}{2\varepsilon}(C_r - \tau_r F_{zr})\right) \right] \hat{v}_{y,r} \\
 &\quad + \left[ \left\{ 1 - \sin\left(\frac{\pi}{2\varepsilon}(C_f - \tau_f F_{zf})\right) \right\} \right. \\
 &\quad \times \left. \left\{ 1 - \sin\left(\frac{\pi}{2\varepsilon}(C_r - \tau_r F_{zr})\right) \right\} \right] \hat{v}_{y,int}. \quad (1)
 \end{aligned}$$

If not in the tolerance region, the terms  $\sin(\pi/2\varepsilon(C_f - \tau_f F_{zf}))$  and  $\sin(\pi/2\varepsilon(C_r - \tau_r F_{zr}))$  are saturated near 0 or 1, depending on the magnitudes of  $C_f$  and  $C_r$ .

### C. Longitudinal Velocity Estimation

The design of the vehicle velocity estimation algorithm introduced in this paper involves the open-loop use of the wheel speed information obtained from the vehicle control area network. Here, the signals from the wheel speed sensors that are attached on each wheel are processed to give the value that is as close as possible to the actual vehicle longitudinal velocity.

First, the left- and right-side wheel speeds are converted to the velocity at the vehicle center line by using the yaw rate term. During acceleration, only the undriven wheel speeds are taken as reliable information, whereas the maximum wheel

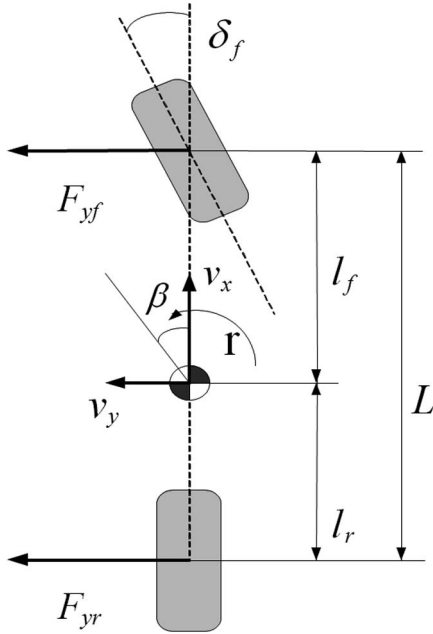


Fig. 4. Bicycle model.

speed value is taken as the vehicle velocity during braking. The result is filtered through the rate limiter, and the limiting value is obtained based on the highest physically allowable limit and the  $x$ -axis accelerometer measurement. The latest value is defined as  $v_{car}$ , and it must be clarified that it is not yet the final estimation of the vehicle longitudinal velocity but is a mere reference value that is used in later parts of this paper.

#### D. Bicycle-Model-Based Observer

The design of the bicycle model observer is based on the following state-space expression of the bicycle model (see Fig. 4):

$$\dot{x} = Ax + Bu \quad (2)$$

where

$$x = \begin{bmatrix} \beta \\ r \end{bmatrix}, \quad u = \delta_f$$

$$A = \begin{bmatrix} a_{11} & a_{12} \\ a_{21} & a_{22} \end{bmatrix} = \begin{bmatrix} -\frac{2(C_f + C_r)}{mv_x} & \frac{-2(C_f l_f - C_r l_r)}{mv_x^2} - 1 \\ -\frac{2(C_f l_f - C_r l_r)}{I_z} & -\frac{2(C_f l_f^2 + C_r l_r^2)}{I_z v_x} \end{bmatrix}$$

$$B = \begin{bmatrix} b_1 \\ b_2 \end{bmatrix} = \begin{bmatrix} \frac{2C_f}{mv_x} \\ \frac{2C_f l_f}{I_z} \end{bmatrix}.$$

Here, the cornering stiffness parameters  $C_f$  and  $C_r$  denote the values obtained by the cornering stiffness adaptation, as explained in Section II-E, and the vertical component of the vehicle motion is assumed to be negligible.

The lateral acceleration of the vehicle is expressed in terms of the longitudinal and lateral velocity and yaw rate as follows:

$$a_y = \dot{v}_y + r v_x. \quad (3)$$

Now, we have

$$v_y = v_x \tan \beta \approx v_x \beta. \quad (4)$$

Therefore, (3) can be altered by using the bicycle model expression of (2) [17] as

$$a_y = a_{11} v_x \beta + (a_{12} + 1) v_x r + b_1 v_x \delta_f. \quad (5)$$

Note that the lateral acceleration dealt in (3) is not necessarily equivalent to the lateral acceleration sensor measurement, because the measurement can be influenced by the vehicle orientation with respect to the earth axes. Either the measurement of the suspension angle from the suspension travel distances (if available) or the open-loop estimation by modeling the vehicle as a spring damper system enables the elimination of the influence of gravity due to the suspension angle on the sensor. At the same time, the effect of the road angle is maintained, because it, in fact, influences the vehicle lateral dynamics. These procedures are shown in the following equation:

$$a_y = a_{y,sensor} + (-g \sin \phi \cos \theta + g \sin \phi' \cos \theta') \quad (6)$$

where

$$\begin{cases} \phi = \phi' + \phi_{sus} \\ \theta = \theta' + \theta_{sus}. \end{cases}$$

The variables  $\phi$ ,  $\phi'$ ,  $\phi_{sus}$ ,  $\theta$ ,  $\theta'$ , and  $\theta_{sus}$  indicate the total roll, static road bank, pure suspension roll, total pitch, static road inclination, and pure suspension pitch angle, respectively. Here, the total roll and pitch angle estimation are obtained based on [22].

The output equation of the bicycle model is given as follows:

$$\hat{y} = C\hat{x} + Du \quad (7)$$

where

$$\hat{y} \triangleq \begin{bmatrix} \hat{r} \\ \hat{a}_y \end{bmatrix}, \quad x \triangleq \begin{bmatrix} \hat{\beta}_{bic} \\ \hat{r} \end{bmatrix}$$

$$C = \begin{bmatrix} 0 & 1 \\ a_{11} v_x & (a_{12} + 1) v_x \end{bmatrix}, \quad D = \begin{bmatrix} 0 \\ b_1 v_x \end{bmatrix}.$$

With the aforementioned expression, the following bicycle-model-based observer is designed:

$$\dot{\hat{x}} = A\hat{x} + Bu + K(y - \hat{y}) \quad (8)$$

where

$$K \triangleq \begin{bmatrix} K_1 & K_2 \\ K_3 & K_4 \end{bmatrix}$$

which leads to the following equation:

$$\begin{aligned} \begin{bmatrix} \dot{\hat{\beta}}_{bic} \\ \dot{\hat{r}} \end{bmatrix} &= \begin{bmatrix} a_{11} - K_2 a_{11} v_{car} & a_{12} - K_1 - K_2 (a_{12} + 1) v_{car} \\ a_{21} - K_4 a_{11} v_{car} & a_{22} - K_3 - K_4 (a_{12} + 1) v_{car} \end{bmatrix} \\ &\times \begin{bmatrix} \hat{\beta}_{bic} \\ \hat{r} \end{bmatrix} + \begin{bmatrix} b_1 - K_2 b_1 v_{car} \\ b_2 - K_4 b_1 v_{car} \end{bmatrix} \delta_f + \begin{bmatrix} K_1 & K_2 \\ K_3 & K_4 \end{bmatrix} \begin{bmatrix} r \\ a_y \end{bmatrix}. \end{aligned} \quad (9)$$

Here,  $\hat{\beta}_{bic}$ ,  $\hat{r}$ ,  $r$ , and  $a_y$  are the estimated side-slip angle, estimated yaw rate, sensor yaw rate measurement, and compensated lateral acceleration measurement, respectively.

The observer gain matrix  $K$  is defined as follows:

$$K = \begin{bmatrix} \frac{I_z(C_f l_f - C_r l_r)}{2C_f C_r (l_f + l_r)^2} p_o^2 - 1 & \frac{1}{v_{car}} \\ -2p_o & \frac{m(C_f l_f^2 + C_r l_r^2)}{I_z(C_f l_f - C_r l_r)} \end{bmatrix} \quad (10)$$

where  $p_o$  is a negative constant. The elements in  $K$  are switched to zero to prevent  $K$  from becoming ill defined with zero denominators.

Choosing the observer gain  $K$ , as shown in (10), guarantees the system stability, and the proof is given in [22].

Finally, using (4), the estimation of the side-slip angle  $\hat{\beta}_{bic}$  leads to the estimated lateral velocity, i.e.,

$$\hat{v}_{y,bic} = v_{car} \tan \hat{\beta}_{bic} \quad (11)$$

where  $\hat{v}_{y,bic}$  is the lateral velocity estimation obtained from the bicycle-model-based observer.

### E. Cornering Stiffness Adaptation

In this paper, vehicle velocity estimation involves the use of a bicycle-model-based observer, and it cannot be denied that the reliability of the bicycle model quickly drops as the tire characteristics turn nonlinear. For this reason, to expand the range of reliable bicycle model use as much as possible, a cornering stiffness adaptation technique is adopted, and it is based on [18].

The adaptive scheme that was designed in [18], however, is modified, and therefore, the burden added by the rapidly changing vertical load is excluded from the adaptation. In other words, if [18] performed the adaptation of the parameters that change as a function of the vertical loads, the modified scheme performs the adaptation of the parameters that are normalized by the vertical loads in advance. Such tactics is applied, because the effect on the cornering stiffness due to the changing vertical load is considered more substantial than other factors.

Setting  $C_f$  and  $C_r$  as the cornering stiffness, they are normalized by the front and rear vertical loads as

$$\bar{C}_f = \frac{C_f}{F_{zf}} \quad (12a)$$

$$\bar{C}_r = \frac{C_r}{F_{zr}}. \quad (12b)$$

Here, the vertical loads are obtained by the open-loop calculation using the vehicle parameters and 6-D IMU information [22].

Now, the normalized variables are divided into the nominal and unknown parts as

$$\frac{1}{\bar{C}_f} = \left( \frac{1}{\bar{C}_f} \right)_n + \zeta_f \quad (13a)$$

$$\frac{1}{\bar{C}_r} = \left( \frac{1}{\bar{C}_r} \right)_n + \zeta_r \quad (13b)$$

where  $(1/\bar{C}_f)_n = F_{zf}(1/C_f)_n$  and  $(1/\bar{C}_r)_n = F_{zr}(1/C_r)_n$  are the nominal values, and  $\zeta_f$  and  $\zeta_r$  are the unknown parts.

Based on the bicycle model, the following relationship is reached:

$$\frac{F_{yf}}{F_{zf}} \left( \left( \frac{1}{\bar{C}_f} \right)_n + \zeta_f \right) - \frac{F_{yr}}{F_{zr}} \left( \left( \frac{1}{\bar{C}_r} \right)_n + \zeta_r \right) = \delta_f - \frac{l_f + l_r}{v_x} r. \quad (14)$$

The lateral tire forces are calculated using the lateral acceleration and yaw rate sensors [22]. Based on (14),  $\zeta$  and  $\hat{\zeta}$  are defined according to the following equations:

$$\begin{aligned} \zeta &\equiv \frac{F_{yf}}{F_{zf}} \zeta_f - \frac{F_{yr}}{F_{zr}} \zeta_r \\ &= \delta_f - \frac{l_f + l_r}{v_x} r - \frac{F_{yf}}{F_{zf}} \left( \frac{1}{\bar{C}_f} \right)_n + \frac{F_{yr}}{F_{zr}} \left( \frac{1}{\bar{C}_r} \right)_n \end{aligned} \quad (15)$$

$$\hat{\zeta} \equiv \frac{F_{yf}}{F_{zf}} \hat{\zeta}_f - \frac{F_{yr}}{F_{zr}} \hat{\zeta}_r. \quad (16)$$

As shown in (15), the state  $\zeta$  conveniently turns out that it can be obtained using the known values of  $\delta_f$ ,  $v_x$ ,  $r$ ,  $F_y$ , and  $F_z$ , on which the adaptation is based.

Applying a low-pass filter to ensure that the system is causal leads to

$$\dot{\zeta} = -\eta \left( \zeta - \frac{F_{yf}}{F_{zf}} \zeta_f + \frac{F_{yr}}{F_{zr}} \zeta_r \right) \quad (17)$$

$$\dot{\hat{\zeta}} = -\eta \left( \hat{\zeta} - \frac{F_{yf}}{F_{zf}} \hat{\zeta}_f + \frac{F_{yr}}{F_{zr}} \hat{\zeta}_r \right) \quad (18)$$

where  $\eta$  is a filter gain.

Now, based on the following adaptation update law, the estimation of the unknown parts of the normalized front and rear cornering stiffness are obtained:

$$\dot{\hat{\zeta}}_f = \eta \eta_f \frac{F_{yf}}{F_{zf}} \varepsilon_n \quad (19)$$

$$\dot{\hat{\zeta}}_r = -\eta \eta_r \frac{F_{yr}}{F_{zr}} \varepsilon_n \quad (20)$$

where  $\eta_f$  and  $\eta_r$  are adaptation gains, and  $\varepsilon_n \triangleq \zeta - \hat{\zeta}$ .

Once the cornering stiffness information is obtained, two pieces of lateral velocity source can be calculated for the observer synthesis. Based on the bicycle model, the following two expressions of the vehicle side-slip angle can be obtained (one expression based on the front tire slip angle, and another expression based on the rear tire slip angle):

$$\beta_f \triangleq \alpha_f - \frac{l_f}{v_x} r + \delta_f \quad (21)$$

$$\beta_r \triangleq \alpha_r + \frac{l_r}{v_x} r. \quad (22)$$

Replacing the variables with those available, with the use of (4), we obtain

$$\hat{v}_{y,f} = v_{car} \tan \hat{\beta}_f \quad (23)$$

$$\hat{v}_{y,r} = v_{car} \tan \hat{\beta}_r \quad (24)$$

with

$$\hat{\beta}_f = \hat{\alpha}_f - \frac{l_f}{v_{car}} r_m + \delta_f = -\frac{F_{yf}}{C_f} - \frac{l_f}{v_{car}} r_m + \delta_f \quad (25)$$

$$\hat{\beta}_r = \hat{\alpha}_r + \frac{l_r}{v_{car}} r_m = -\frac{F_{yr}}{C_r} + \frac{l_r}{v_{car}} r_m. \quad (26)$$

Details on the background principles are shown in [18]. Furthermore, the stability analysis of the aforementioned system is omitted, because it is not much different from what is noted in [18].

#### F. Pseudointegral Kinematic Estimation

Kinematic estimation has its base on the following model of the vehicle dynamics:

$$\dot{v}_x = a_x + r \cdot v_y - q \cdot v_z + g \cdot \sin \theta \quad (27a)$$

$$\dot{v}_y = a_y - r \cdot v_x + p \cdot v_z - g \cdot \sin \phi \cdot \cos \theta \quad (27b)$$

$$\dot{v}_z = a_z + q \cdot v_x - p \cdot v_y - g \cdot \cos \phi \cdot \cos \theta \quad (27c)$$

where  $a_x$ ,  $a_y$ ,  $a_z$ ,  $p$ ,  $q$ , and  $r$  are the longitudinal, lateral, vertical accelerations, roll rate, pitch rate, and yaw rate, respectively, all obtained by the 6-D IMU.

The time derivative of the velocities of each vehicle axis is expressed in terms of the 6-D sensor signals and the total roll and pitch angles. Here, all the terms that appear in the kinematic model refer to the values taken at the CG. The kinematic model surely involves the issue of high sensitivity to sensor error, because all of the values measured by the 6-D IMU are fully and directly used to calculate the vehicle states. However, as long as this issue can be overcome, the kinematic model is effective in estimating the vehicle states, because it does not require any secondary identification of the unknown vehicle parameters and properties.

To eliminate any possible drift phenomena that may arise from the integration of the kinematics equations as much as possible, the concept of the pseudointegration is introduced. Because it is apparent that errors accumulate during integration, unless the sensor measurements are completely free from the offset error, integration must be repressed whenever it is not necessary. Here, the transient factor (TF) is defined to indicate that the vehicle is exhibiting a transient state in its dynamics [22] as where  $x_1 = a_x$ ,  $x_2 = a_y$ ,  $x_3 = a_z$ ,  $x_4 = p$ ,  $x_5 = q$ ,  $x_6 = r$ ,  $x_7 = v_{car}$ , and  $b_i$  are the positive weighting factors for each term to be tuned. Here, values of the variables  $x_1$  to  $x_6$  are the sensor measurements.  $b_8$  and  $\sigma_{v_x}$  are also positive tuning coefficients, and the related terms will ensure that  $TF = 0$

when  $v_{car} = 0$  for a time period  $\Delta t_8$ . This condition applies under the assumption that the vehicle states do not need to be estimated if the vehicle is at a complete stop. TF basically takes the form of the weighted sum of the sensor signal amplitudes; therefore, its value is increased with much transient motion, and *vice versa*.

The nonlinear condition mentioned in (28), shown at the bottom of the page, refers to the nonlinear tire characteristics. It is the condition in which the tire cornering stiffness has significantly decreased relative to those in the condition where the linear tire model fits quite well. This nonlinear condition is characterized by the states in which any one of the following conditions applies [22]:

$$(a) \frac{\int_t^{t+\Delta t_9} \left( C_f - \frac{\int_t^{t+\Delta t_9} C_f d\tau}{\Delta t} \right)^2 d\tau}{\Delta t} > \sigma_{C_f} \quad (29)$$

$$(b) \frac{\int_t^{t+\Delta t_{10}} \left( C_r - \frac{\int_t^{t+\Delta t_{10}} C_r d\tau}{\Delta t} \right)^2 d\tau}{\Delta t} > \sigma_{C_r} \quad (30)$$

$$(c) C_f < \eta_f \left( \left( \frac{1}{C_f} \right)_n \right)^{-1} \text{ or } C_r < \eta_r \left( \left( \frac{1}{C_r} \right)_n \right)^{-1}$$

$$\text{when } \frac{\int_t^{t+\Delta t_{11}} \left( \delta_f - \frac{\int_t^{t+\Delta t_{11}} \delta_f d\tau}{\Delta t} \right)^2 d\tau}{\Delta t} > \sigma_{\delta_f} \quad (31)$$

where  $\eta_f$ ,  $\eta_r$ ,  $\sigma_{C_f}$ ,  $\sigma_{C_r}$ , and  $\sigma_{\delta_f}$  are the positive tuning parameters, and  $\eta_f$ ,  $\eta_r$  are set to satisfy  $0 < \eta_f < 1$  and  $0 < \eta_r < 1$ , respectively. Equations (29) and (30) each indicate that the variance of front and rear cornering stiffness values are higher than the established threshold  $\sigma_{C_f}$  and  $\sigma_{C_r}$ . It is implied that the cornering stiffness values are vigorously changing; hence, the tire characteristics are unlikely to be linear. Now, (31) indicates that either the front or the rear cornering stiffness value is lower than a certain portion of the nominal (thus, the linear tire model) cornering stiffness value. This case clearly states that the vehicle tires are exhibiting a nonlinear characteristic. Note that an additional condition as a function of steering angle input is attached to (31). The reasoning behind this attachment is to ensure that the updated cornering stiffness values are obtained under the persistent excitation condition [23].

The stability factor (SF) is a complementary concept of TF. In other words, SF and TF always sum up to 1, as shown in the following expression:

$$SF = 1 - TF. \quad (32)$$

$$TF = \begin{cases} \text{sat} \left( \frac{b_8 \int_t^{t+\Delta t_8} x_7 d\tau}{\Delta t} - \sigma_{v_x} \right), & \text{nonlinear condition} \\ \text{sat} \left\{ \text{sat} \left( \frac{b_8 \int_t^{t+\Delta t_8} x_7 d\tau}{\Delta t} - \sigma_{v_x} \right) \sum_{i=1}^7 \left\{ \frac{b_i \int_t^{t+\Delta t_i} \left( x_i - \frac{\int_t^{t+\Delta t_i} x_i d\tau}{\Delta t} \right)^2 d\tau}{\Delta t} \right\} \right\}, & \text{otherwise} \end{cases} \quad (28)$$

Here, the nature of the vehicle dynamic stability referred by the stability factor is stricter than what the steady state implies. Although a steady-state condition only implies that the vehicle motion is not going under a changing phase, the stable condition in this paper additionally implies that the vehicle tires exhibit linear characteristics. For example, a vehicle that smoothly and constantly slips sideway on the icy surface without changing its orientation or velocity is likely to be in a steady state but unlikely to have a high SF.

Putting (27) into the matrix form gives the following state-space equations of the vehicle kinematics:

$$\begin{bmatrix} \dot{v}_x \\ \dot{v}_y \\ \dot{v}_z \end{bmatrix} = \begin{bmatrix} 0 & r & -q \\ -r & 0 & p \\ q & -p & 0 \end{bmatrix} \cdot \begin{bmatrix} v_x \\ v_y \\ v_z \end{bmatrix} + \begin{bmatrix} a_x \\ a_y \\ a_z \end{bmatrix} + g \begin{bmatrix} \sin \theta \\ -\sin \phi \cdot \cos \theta \\ -\cos \phi \cdot \cos \theta \end{bmatrix}. \quad (33)$$

Because  $v_{car}$  is used as the longitudinal velocity in the pseudointegral kinematic estimation part, the first row kinematics that deals with the time derivative of the longitudinal velocity is unnecessary. Hence, by taking only (27b) and (27c) and substituting the variables with those available, the following expression is reached, and in doing so, the pseudointegration system is designed to incorporate TF and SF; therefore, high TF encourages pure integration, whereas high SF stagnates the integration to hold the estimated lateral velocity at  $\hat{v}_{y,bic}$  and the estimated vertical velocity at 0

$$\dot{v}_{y,int}^* = a_{y,m} - r_m \cdot v_{car} + p_m \cdot \hat{v}_{z,int} - g \cdot \sin \hat{\phi} \cdot \cos \hat{\theta} \quad (34)$$

$$\dot{v}_{z,int}^* = a_{z,m} + q_m \cdot v_{car} - p_m \cdot \hat{v}_{y,int} - g \cdot \cos \hat{\phi} \cdot \cos \hat{\theta} \quad (35)$$

$$\hat{v}_{y,int} = TF \cdot \hat{v}_{y,int}^* + SF \cdot \hat{v}_{y,bic} \quad (36)$$

$$\hat{v}_{z,int} = TF \cdot \hat{v}_{z,int}^* \quad (37)$$

where  $\hat{v}_{y,int}$  and  $\hat{v}_{z,int}$  are the lateral and vertical velocities estimated by pseudointegration;  $v_{car}$  is the longitudinal velocity estimation based on the wheel dynamics;  $\hat{\phi}$  and  $\hat{\theta}$  are the estimated roll and pitch angles; and  $a_{y,m}$ ,  $a_{z,m}$ ,  $p_m$ ,  $q_m$ , and  $r_m$  are the sensor measurements.

The aforementioned system performs the integration of  $\hat{v}_{y,int}^*$  and  $\hat{v}_{z,int}^*$ , with the sensor measurements that may involve error. Although this case may lead to the estimated velocities to gradually drift away as time elapses, the stabilization of the vehicle motion quickly returns and holds the estimated velocities at  $\hat{v}_{y,bic}$  and 0 to correct the drift error. Intuitive analysis of the aforementioned system thus tells that the system is stable, as long as the bicycle model observer is stable, which has been proven [17].

### G. Principal Kinematic Observer

An observer that uses the kinematics equations of motion is implemented as the last part of the entire observer structure to process the signals obtained from other preliminary components in an integrated manner. Here, analogous to the

pseudointegral kinematic estimation structure, this observer fully and directly takes advantage of the measurements from the 6-D IMU but, this time, along with the reference lateral velocity information  $\hat{v}_{y,ref}$  obtained from the final result of the observer synthesis. In other words, the kinematic observer that is relatively free from the signal drift problem, is achieved through  $\hat{v}_{y,ref}$ , which has maximized the advantage of using the bicycle model by the observer synthesis.

The principal kinematic observer operates based on the aforementioned kinematic equations of motion, as shown in (27). Adding the observer feedback term to (27), the following observer design can be reached to give the final vehicle velocity estimations:

$$\dot{x}_{pko} = A_{pko}x_{pko} + L + K_{ki}(y_{ref} - y_{pko}) \quad (38)$$

$$y_{pko} = C_{pko}x_{pko} \quad (39)$$

where

$$x_{pko} = \begin{bmatrix} \hat{v}_x \\ \hat{v}_y \\ \hat{v}_z \end{bmatrix}, \quad A_{pko} = \begin{bmatrix} 0 & r_m & -q_m \\ -r_m & 0 & p_m \\ q_m & -p_m & 0 \end{bmatrix}$$

$$L = \begin{bmatrix} a_{x,m} + g \sin \hat{\theta} \\ a_{y,m} - g \sin \hat{\phi} \cdot \cos \hat{\theta} \\ a_{z,m} - g \cos \hat{\phi} \cdot \cos \hat{\theta} \end{bmatrix}$$

$$C_{pko} = I, \quad y_{ref} = \begin{bmatrix} v_{car} \\ \hat{v}_{y,ref} \\ 0 \end{bmatrix}$$

$$K_{ki} = \begin{bmatrix} k_1 & k_2 & k_3 \\ k_4 & k_5 & k_6 \\ k_7 & k_8 & k_9 \end{bmatrix} = \begin{bmatrix} \xi_x & r_m & -q_m \\ -r_m & \xi_y & p_m \\ q_m & -p_m & \xi_z \end{bmatrix}.$$

Here,  $\xi_x$ ,  $\xi_y$ , and  $\xi_z$  are positive constants.

For the  $x$ -axis kinematics, the longitudinal velocity  $v_{car}$  that has been computed through wheel dynamics is taken for the observer reference. By doing so, the objectives of improving the principal kinematic observer estimation accuracy by resolving its possible issue of signal drift and improving the longitudinal velocity estimation of  $v_{car}$  by not only depending on the wheel dynamics but by using the 6-D sensor information as well can simultaneously be fulfilled.

In a similar context, the use of  $\hat{v}_{y,ref}$  for the  $y$ -axis observer feedback not only blocks the drift of the estimated results of the principal kinematic observer but also increases the accuracy of the lateral velocity estimation relative to that of  $\hat{v}_{y,ref}$  itself by enabling fine estimation and eliminating the noise without causing any phase lag issue. This case is further discussed with respect to the experimental results in the analysis section.

With regard to the  $z$ -axis kinematics, the reference vertical velocity is simply taken to be zero. Aside from the purpose of preventing the integration drift issue, this is accounted by the small magnitude of the vertical velocity and the fact that the long-term  $z$ -axis behavior of the vehicle evens out to zero vertical velocity.

TABLE I  
TEST VEHICLE SPECIFICATION

| Tucson ix 2WD Gasoline Theta II 2.0 Specification |                             |       |       |      |       |
|---|-----------------------------|-------|-------|------|-------|
| Feature   |                             | Front |       | Rear |       |
|   |                             | Left  | Right | Left | Right |
| Dimension [mm]                                    | Wheelbase                   | 2640  |       |      |       |
|   | Overhang                    | 800   |       | 890  |       |
|   | Track                       | 1585  |       | 1586 |       |
|   | Overall Length              | 4410  |       |      |       |
|   | Overall Width               | 1820  |       |      |       |
|   | Height (unloaded)           | 1655  |       |      |       |
| Weight [kgf]                                      | Curb weight                 | 450   | 417   | 326  | 330   |
|   |                             | 867   |       | 656  |       |
|   |                             | 1523  |       |      |       |
|   | Gross vehicle weight (2 up) | 487   | 458   | 360  | 368   |
|   |                             | 945   |       | 728  |       |
|   |                             | 1673  |       |      |       |
| Wheel radius [mm]                                 | 336                         | 338   | 340   | 340  |       |
|   | 337                         |       | 340   |      |       |

Stability can easily be proved by investigating (38) and (39). Some algebraic manipulation and substitution of these relationships lead to the following expression:

$$\begin{aligned}
 \dot{x}_{pko} &= A_{pko}x_{pko} + L + K_{ki}(y_{ref} - y_{pko}) \\
 &= A_{pko}x_{pko} + L + K_{ki}(y_{ref} - C_{pko}x_{pko}) \\
 &= (A_{pko} - K_{ki}C)x_{pko} + L + K_{ki}y_{ref}. \quad (40)
 \end{aligned}$$

Here, it can simply be found that

$$\begin{aligned}
 &A_{pko} - K_{ki}C \\
 &= \begin{bmatrix} 0 & r_m & -q_m \\ -r_m & 0 & p_m \\ q_m & -p_m & 0 \end{bmatrix} - \begin{bmatrix} \xi_x & r_m & -q_m \\ -r_m & \xi_y & p_m \\ q_m & -p_m & \xi_z \end{bmatrix} \cdot I \\
 &= \begin{bmatrix} -\xi_x & 0 & 0 \\ 0 & -\xi_y & 0 \\ 0 & 0 & -\xi_z \end{bmatrix} \quad (41)
 \end{aligned}$$

is strictly Hurwitz. Hence, the error dynamics of the principal kinematic observer is asymptotically stable, assuming that  $y \approx y_{ref}$ .

### III. EXPERIMENTAL RESULTS

#### A. Test Environments

The experiments are conducted using a real production sport utility vehicle, i.e., the Hyundai Tucson ix, to verify the velocity

TABLE II  
INSTRUMENT-MOUNTING POSITIONS

| Distance between instruments |                         | Distance [mm] |
|------------------------------|-------------------------|---------------|
| Length (X-axis)              | RT3100~rear axle center | 1000          |
|                              | RT3100~6D IMU           | 930           |
| Height (Z-axis)              | RT3100~antenna          | 600           |
|                              | RT3100~6D IMU           | 430           |

TABLE III  
TEST SCENARIOS

| Case     | Driver Control       | Bank             | Incline                         | Road condition |
|----------|----------------------|------------------|---------------------------------|----------------|
| Case I   | Sine steer           | none             | none                            | Dry asphalt    |
| Case II  | DLC                  | none             | none                            | Dry asphalt    |
| Case III | Circle turn          | none             | none                            | Wet asphalt    |
| Case IV  | Bumpy road           | sinusoidal       | sinusoidal                      | Dry asphalt    |
| Case V   | J-turn               | none             | none                            | Wet asphalt    |
| Case VI  | Spin out             | none             | none                            | Snow           |
| Case VII | Bank turn sine steer | 0→20→0→20<br>→0° | Irregular (depends on position) | Dry asphalt    |

estimation performance. Table I gives the specification of the vehicle used for the experiments. The proposed observer ran on the basis of 5 ms as its sampling time, and no issue with regard to the computation burden was found.

The most affordable class of 6-D IMU from Analog Devices Inc. is used for the observer algorithm. A set of ADW22307 is chosen as the gyroscope, and a set of ADXL103 is chosen as the accelerometer.

For verification, the RT3100 model, which is a high-accuracy differential Global Positioning System (DGPS)-based vehicle dynamics testing tool from the RT3000 family of Oxford Technical Solutions Ltd., is used to measure the actual vehicle states. The detailed specification data of the aforementioned models are available at the corresponding companies. The coordination of these sensors is given in Table II.

Table III shows the list of scenarios by which the experiments are performed. Through variation of conditions and vehicle maneuvers, verification of the estimation performance under a wide range of situations is made possible.

#### B. Experiment Case I

The first case of the experiment is a severe sine steer maneuver on the dry asphalt. A continued series of sine steers can invoke a fairly high amount of vehicle roll and side slip. Under this condition, the side-slip angle is accurately estimated, as shown in Fig. 5.

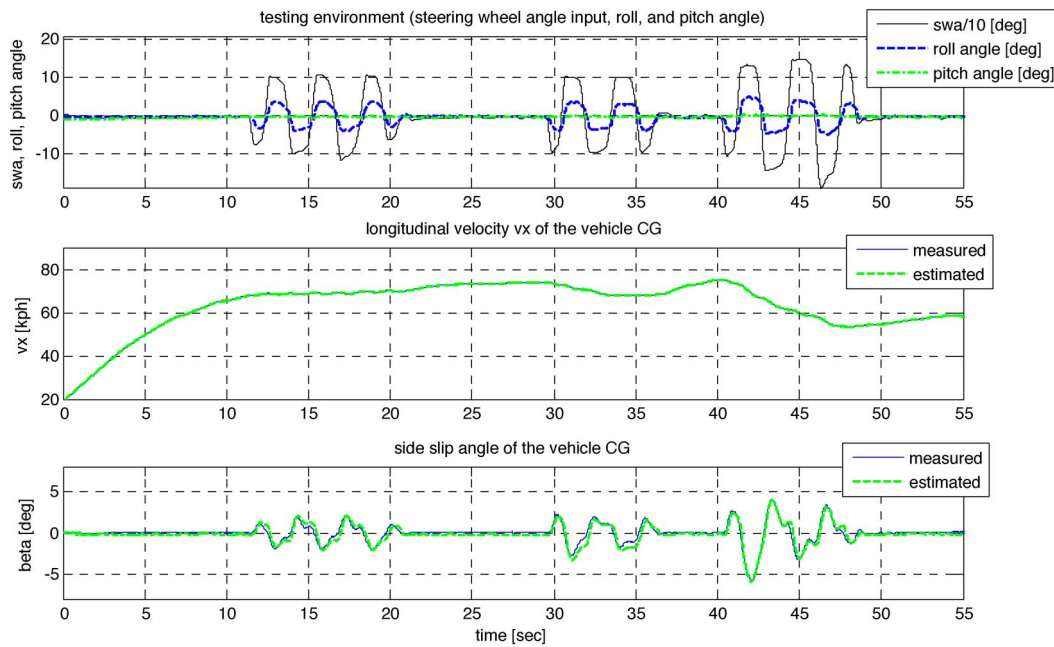


Fig. 5. Sine steer test result for longitudinal velocity and side-slip angle estimation.

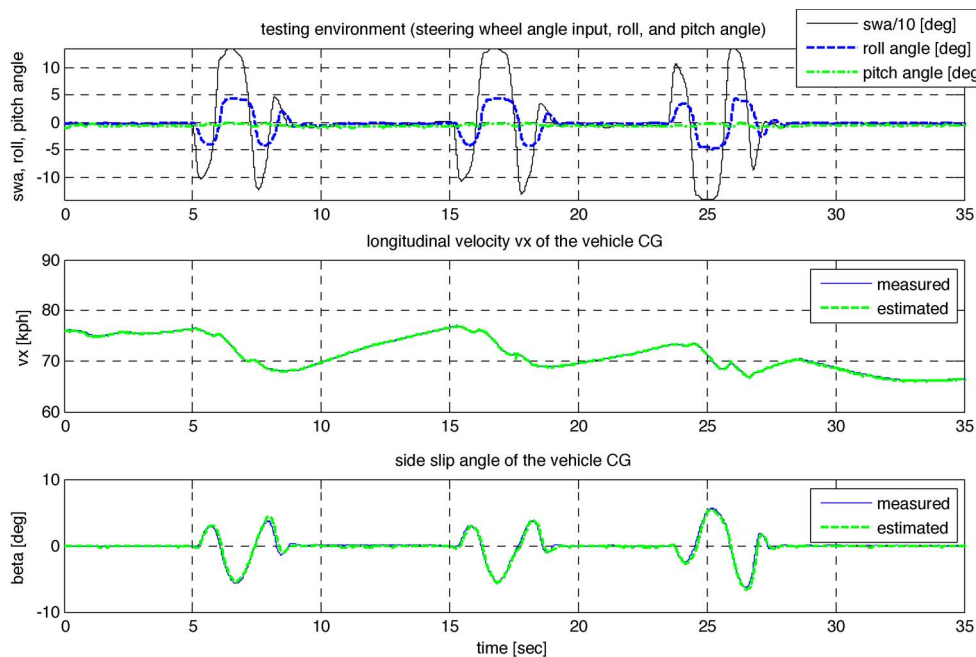


Fig. 6. DLC test result for longitudinal velocity and side-slip angle estimation.

### C. Experiment Case 2

Similar to the previous case, the vehicle is driven on the flat dry asphalt. In this test, the driver mimicked the steering as in the situation of dodging a hindrance; therefore, the vehicle abruptly changes its lane and quickly comes back.

Three sets of the aforementioned maneuvers are done to prove the estimation performance both during the transient and steady states before and after the double lane change (DLC). The proposed observer shows an accurate tracking performance, as shown in Figs. 6–11.

Fig. 12 shows the cornering stiffness adaptation result of one of the sets of DLC described in Fig. 6. It is shown here that the cornering stiffness indeed drops as the front and rear tires show deviations from the linear tire model.

As aforementioned, the observer synthesis resides on the principle of adjusting the weighting factors among the four types of references. These factors are obtained based on the cornering stiffness adaptation values, which are already shown in Fig. 12. Fig. 13 again takes the DLC maneuver as an example. When the vehicle is in a cruising condition without much road disturbance, the bicycle model observer is highly reliable,

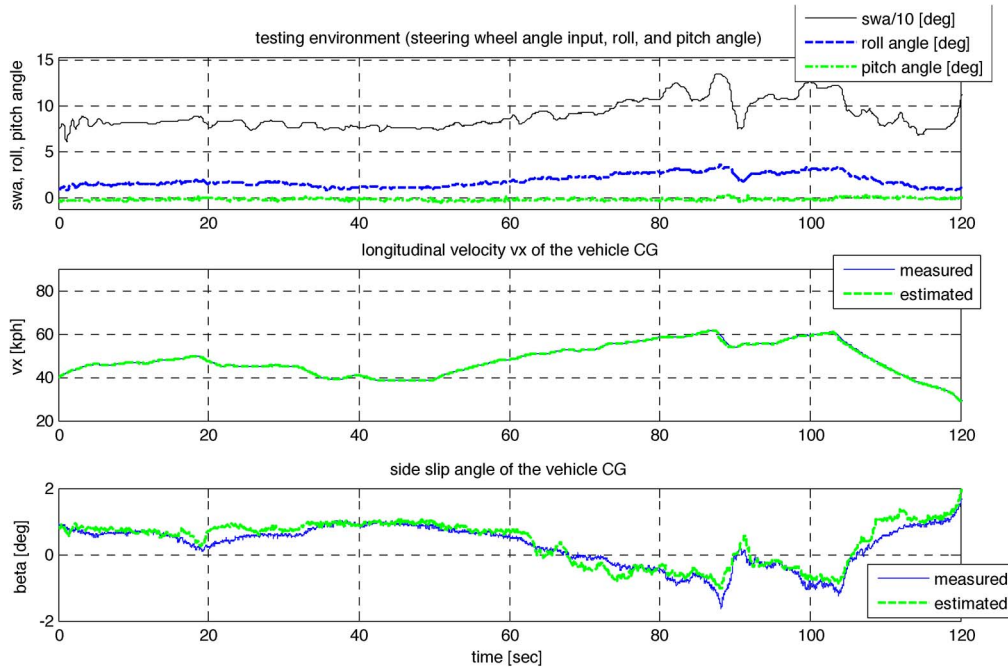


Fig. 7. Circle-turn test result for longitudinal velocity and side-slip angle estimation.

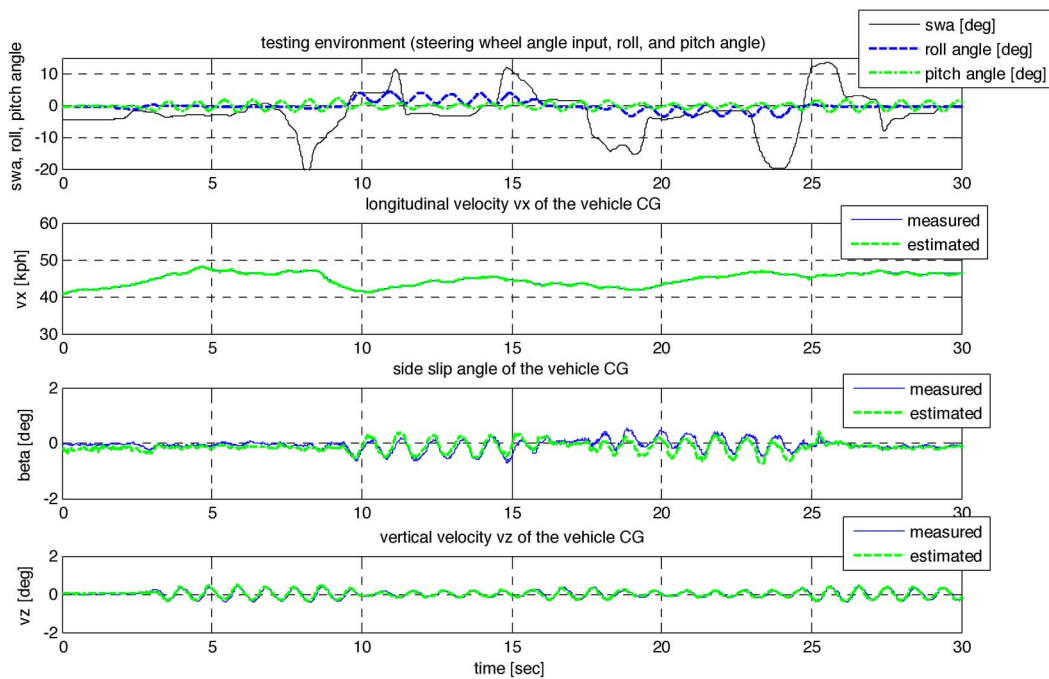


Fig. 8. Bumpy-road test result for longitudinal velocity, side-slip angle, and vertical velocity estimation.

and the weighting factor for the bicycle model observer is close to 1. Now, when the vehicle begins its severe lane change, the weighting factor for the bicycle model observer suddenly drops, and the factors for other references rise. Because a severe DLC may cause both front and rear tires to exhibit nonlinear characteristics, the weighting factor for the pseudointegration shoots up to induce the observer to rely more on the sensor kinematics. When the lane change maneuver is done and the vehicle goes into a stable steady state, both cornering stiffnesses rise back to their linear nominal values, which result in the

immediate rise in the weighting factor for the bicycle model observer and the opposite for the others.

Fig. 14 displays a bundle of lateral velocity reference sources— $v_y$  obtained from pseudointegration, front tire dynamics, rear tire dynamics, and bicycle model observer—along with the actual lateral velocity and  $\hat{v}_{y,ref}$ , the multiple-observer estimation of the reference sources. It is shown in this plot that this combination of the four sources of reference gives the best lateral velocity reference, which can be used in the principal kinematic observer, which follows the observer synthesis.

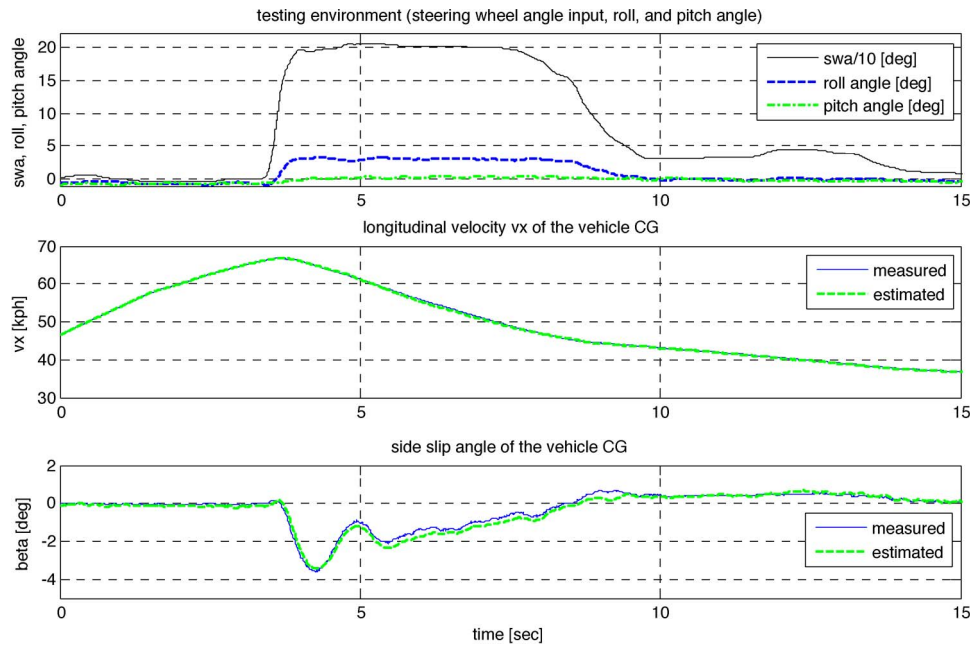


Fig. 9. J-turn test result for longitudinal velocity and side-slip angle estimation.

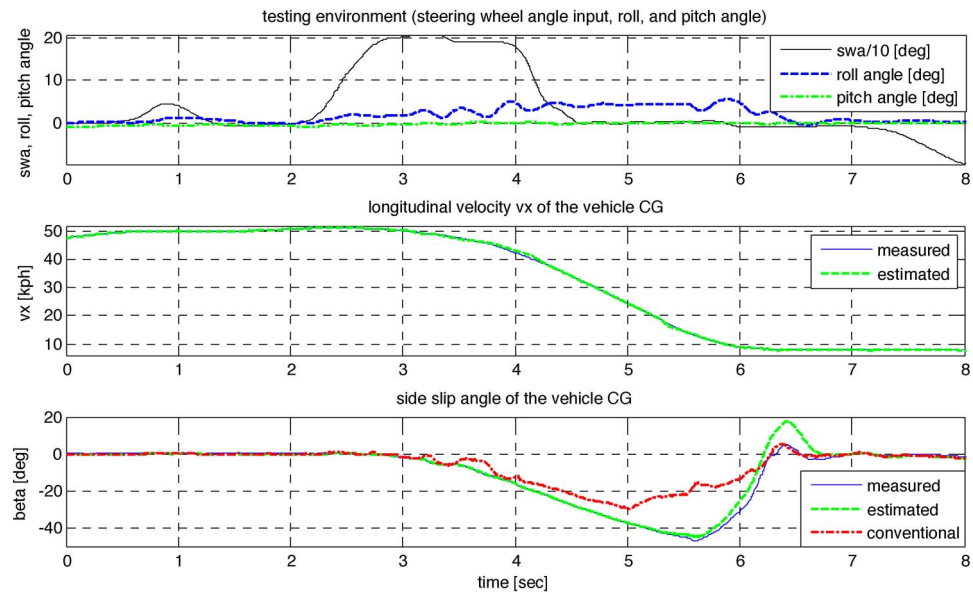


Fig. 10. Spin-out test result for longitudinal velocity and side-slip angle estimation. Comparison of the side-slip angle estimation performance of this paper and conventional work to the measured data.

The principal kinematic observer is designed to have the form of a first-order Kalman filter, which uses the lateral velocity estimation of the multiple-observer synthesis as the lateral dynamics reference. Notice how the result of the observer synthesis involves much noise and rough signals. This roughness in signals is inevitably generated by splicing the reference sources, depending on the cornering stiffness values obtained from the adaptation and vehicle axle vertical loads that already contain much noise in the first place.

Heavily placing a low-pass filter to get rid of the noise is not an option, because such a design results in phase lag. Instead, inducing the noisy reference signals to be filtered by the principal kinematic observer can lead to an accurate

estimation. The estimation result of the vehicle lateral velocity obtained by such a method is compared to the raw observer synthesis result and the measured signal in Fig. 15, and it is apparent that the accuracy is maintained in the final estimation without causing phase lag.

Fig. 16 compares the lateral velocity estimations obtained by the cornering stiffness adaptation [18] and the proposed observer. The estimation algorithms are applied onto the test vehicle that goes under a severe DLC. During this maneuver, the tires exhibit nonlinear characteristics, and the performance of the estimation purely by using the bicycle model is limited, even with the parameter uncertainty compensation through cornering stiffness adaptation. This is verified by the decreased

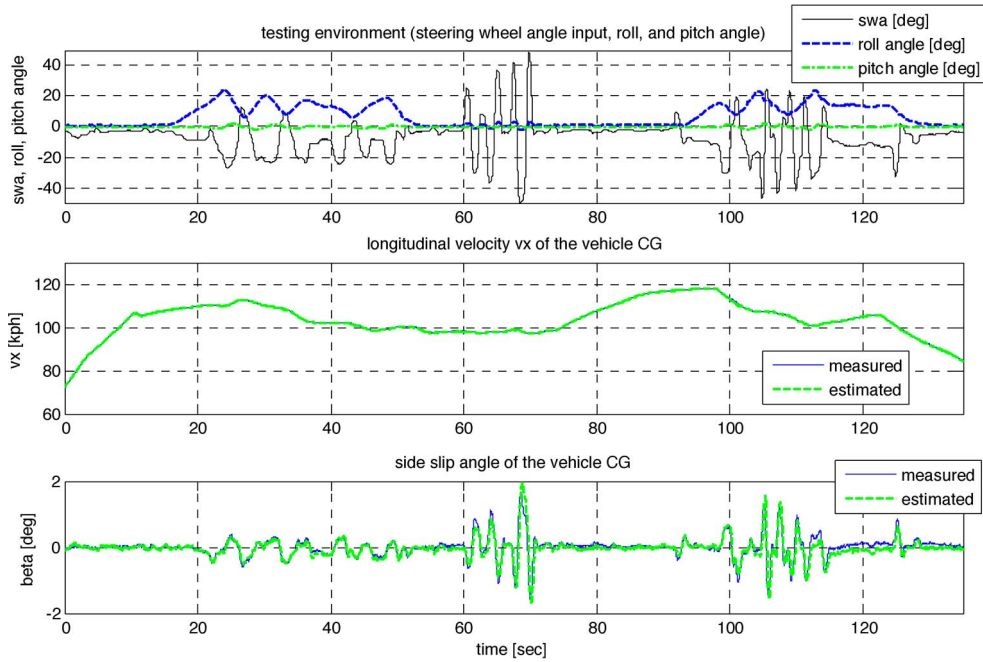


Fig. 11. Bank-turn sine steer test result for longitudinal velocity and side-slip angle estimation.

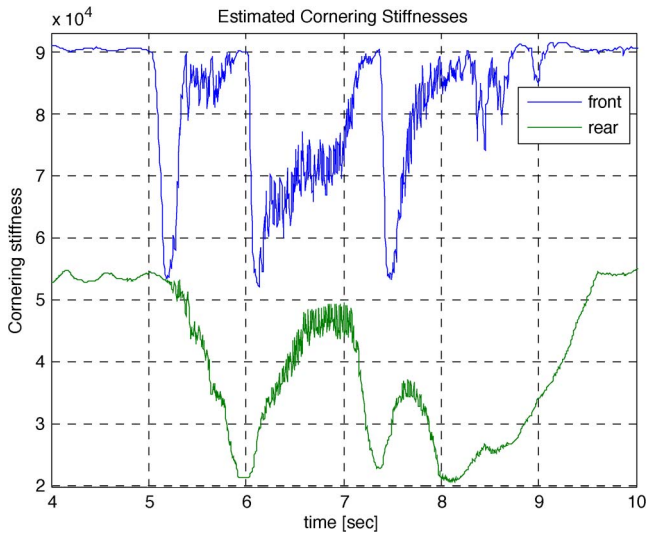


Fig. 12. Cornering stiffness adaptation results for the DLC test.

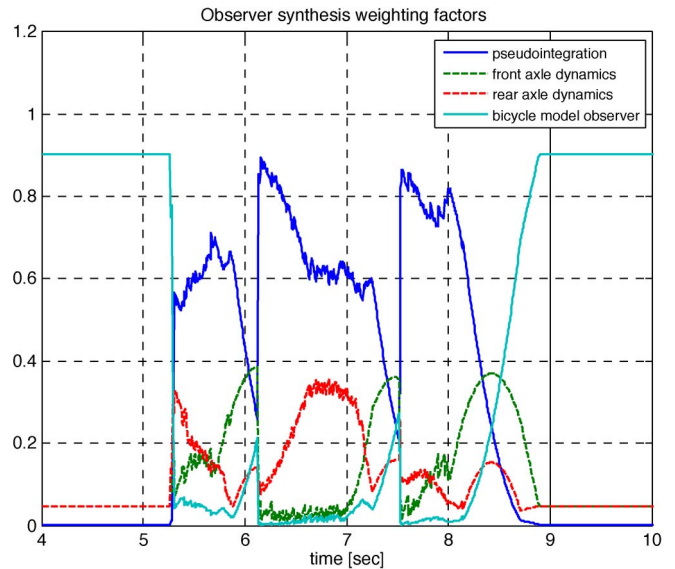


Fig. 13. Observer synthesis weighting factors for DLC.

estimation accuracy of the conventional observer whenever the lateral velocity grows higher than  $1 \sim 2$  m/s. On the other hand, the proposed observer with the observer synthesis effectively chooses to exploit the 6-D IMU through pseudointegration in the highly nonlinear regions; therefore, the lateral velocity estimation is robust to the sources of disturbance, as seen from the bicycle model perspective.

*D. Experiment Case 3*

To more clearly visualize the weighting-factor-adjusting procedures in observer synthesis, the vehicle is gradually led into an understeer condition. Here, the understeer is intentionally made by constantly turning the vehicle in a circular track and increasing its velocity at the same time.

While the vehicle is turning a constant radius circle, the side-slip angle is positive up to around 60 s, but it soon changes its sign and becomes negative. This case can be accounted by the CG, which longitudinally and laterally moves in the direction of cornering in the lack of vehicle tangential velocity on the curve. When the vehicle speeds up, however, the effect of the vehicle inertia that drives the vehicle outward from the curve outgrows the aforementioned effect and causes the vehicle to slip sideways in the opposite direction of cornering. This phenomenon is fairly accurately estimated, as shown in Fig. 7.

As expected, the weights of the observer synthesis show that the major contribution of the bicycle-model-based observer gradually shifts to the contribution of the rear wheel dynamics. This makes sense, because the increase in the vehicle understeer

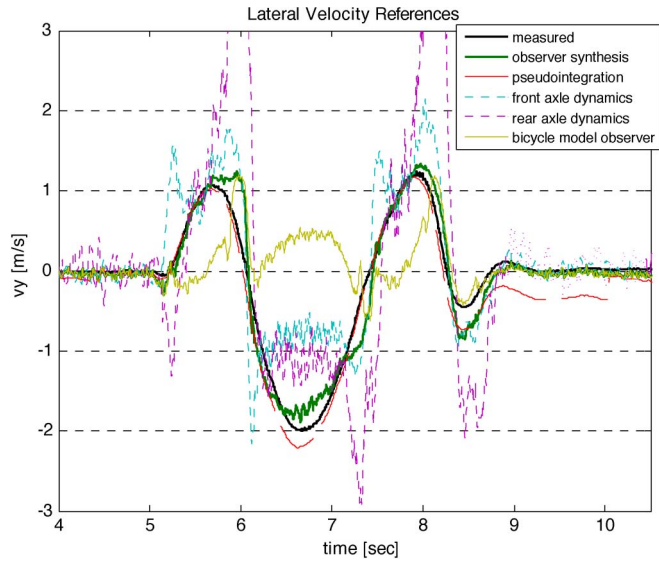


Fig. 14. Comparison of the four lateral velocity inputs for the observer synthesis and its result for the measured lateral velocity.

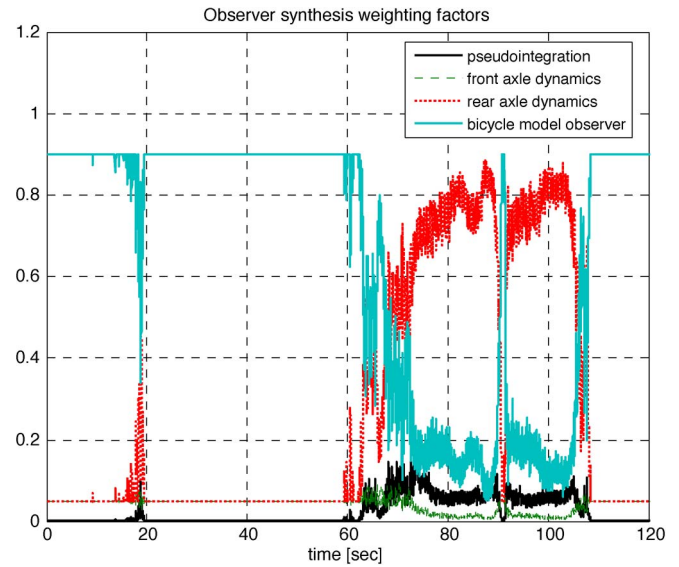


Fig. 17. Observer synthesis weighting factors for a circle turn.

indicates the decrease in the front tire cornering stiffness, which makes it more favorable to use the rear wheel dynamics—which is still relatively linear—for the lateral velocity estimation. Such a phenomenon is accurately reflected in Fig. 17, where the weighting factors for the bicycle model observer decreases, whereas the weighting factors for the rear axle dynamics increases as the understeer proceeds from around 60 s.

E. Experiment Case 4

Vertical velocity estimation is most required for the effective CDC system. Because the most important purpose of such semiactive suspension control is for the increase in ride quality, the vertical velocity estimation performance is tested on the road terrain, which can provide sinusoidal excitation onto the tires.

As shown in Fig. 8, vehicle velocities of all axes are simultaneously estimated without any delay or phase lag. This suggests a promising possibility of applying the semiactive damper control system by exploiting the real-time estimation of the vertical velocity.

F. Experiment Case 5

This scenario deals with a sudden J-turn on the wet road condition, which is initiated at the longitudinal velocity of 70 km/h. As shown in Fig. 9, the observer effectively estimates the sudden change of the side-slip angle, even under the effect of the vehicle roll.

G. Experiment Case 6

The vehicle is maneuvered into a complete spin-out condition on a slippery road, and its test result is shown in Fig. 10.

Although it is true that this type of severe condition must be avoided as much as possible by applying the electronic vehicle safety control technologies, this spin-out test is performed to show how robust the estimation performance is, even up to the

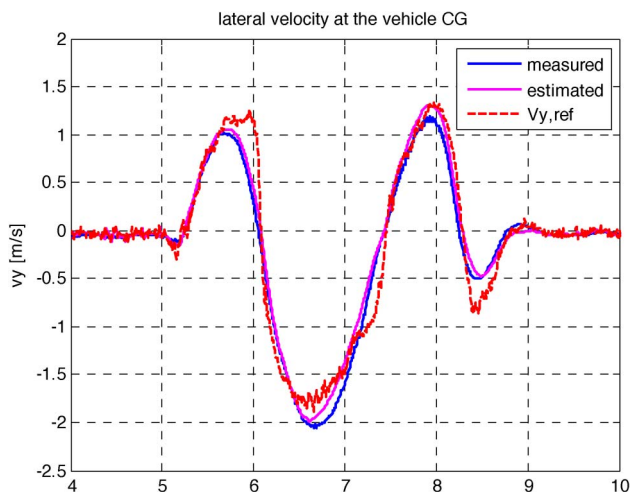


Fig. 15. Comparison of the raw observer synthesis result and the final  $v_y$  estimation by principal kinematic observer to the measured data.

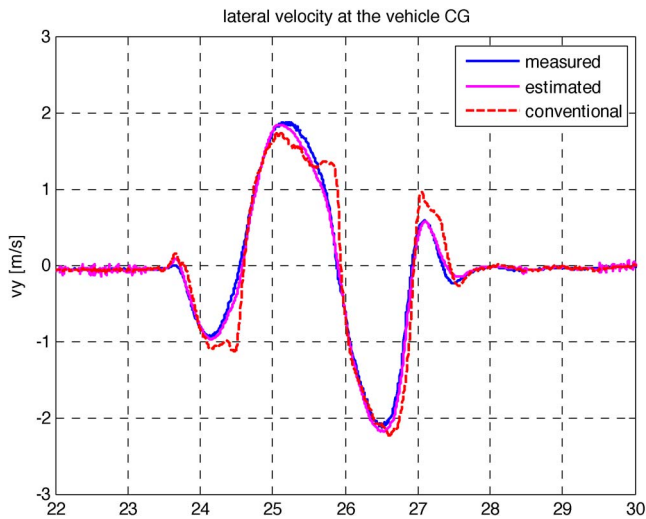


Fig. 16. Comparison of the new and conventional observer estimation performances.

condition that involves the side-slip angle of more than  $40^\circ$ . Through the cost effective 6-D IMU, accurate vehicle lateral velocity estimation has been made possible, which most likely would not be achieved by the use of the bicycle model alone.

At around 6 s and onward, the side-slip angle estimation error instantly mounts up to  $13^\circ$ . This case, however, carries less importance, because it is caused by a low value of longitudinal velocity, which is in the denominator for the side-slip angle calculation. Compared with the fairly accurate estimation result of the suggested observer, the lateral velocity estimation result of the conventional observer [18] is more inaccurate and noisy, particularly when the side-slip angle is large.

#### H. Experiment Case 7

To consider the effect of a static bank and an inclination angle that exist in the road terrain, the vehicle is driven onto a high-speed circuit, which comprises the corners that include the static bank angle of up to  $20^\circ$ . By performing the sine steer maneuver on this severe bank, the vehicle experiences biased acceleration and side slip, as well as the effect of the longitudinal inclination angle, depending on the orientation of the vehicle body on the banked course.

By successfully separating the lateral acceleration value with respect to the road surface on which the vehicle is running, the suggested algorithm effectively estimates the side-slip angle, even on the severe bank angle, as shown in Fig. 11.

### IV. CONCLUSION

This paper has proposed a novel method of effectively combining the role of the bicycle-model-based observer and the kinematic observer to estimate the vehicle velocities of all axes. Making use of a 6-D IMU of the most affordable cost range and discarding the dependency on GPS, the suggested velocity observer exhibits robust and accurate estimation performance, regardless of the possible influence of sensor error and highly nonlinear tire characteristics. In summary, previous studies involved the tradeoff between severely nonlinear tire dynamics estimation accuracy and estimation drift issue settlement, whereas this paper has provided both estimation accuracy in highly transient state and freedom from signal drifting through the multiple-observer approach and its synthesis. In addition, although previous studies did not provide vehicle velocity estimations on all three axes, this paper has contributed in the simultaneous estimation of  $v_x$ ,  $v_y$ , and  $v_z$ .

With numerous real car-based experiments, the velocity estimation performance of the proposed observer is tested and verified to be robust. The experiments are conducted under various conditions, and therefore, the suggested algorithm is ready for the production car application.

### APPENDIX

Figs. 18–20 show photographs of the test vehicle, the RT3100, and the test-drive course at the Hyundai Motor Company Namyang Main R&D Center, respectively.



Fig. 18. Test vehicle.



Fig. 19. RT3100.



Fig. 20. Test-drive course (Hyundai Motor Company Namyang Main R&D Center).

### ACKNOWLEDGMENT

The authors would like to thank S. H. You, J. Y. Seo, and S. G. Kang of Hyundai Motor Company for their tireless efforts in developing the contents and Hyundai Motor for sponsoring the vehicle, 6-D IMU, and RT3100. This paper has its origin in the X-by-Wire Project, without which this paper could not have been completed. This work was also supported by the

National Research Foundation of Korea (NRF) grant funded by the Korea government (MEST) (No. 2012-0000991).

## REFERENCES

- [1] S. Kimbrough, "Coordinated braking and steering control for emergency stops and accelerations," in *Proc. WAM ASME*, Atlanta, GA, 1991, pp. 229–244.
- [2] A. Nishio, K. Tozu, H. Yamaguchi, K. Asano, and Y. Amano, "Development of vehicle stability control system based on vehicle side-slip angle estimation," presented at the Soc. Autom. Eng. (SAE) World Congr., Detroit, MI, 2001, SAE Tech. Paper 2001-01-0137.
- [3] O. Mokhiamar and M. Abe, "Active wheel steering and yaw moment control combination to maximize stability as well as vehicle responsiveness during quick lane change for active vehicle handling safety," in *Proc. Inst. Mech. Eng. D: J. Autom. Eng.*, 2002, vol. 216, pp. 115–124.
- [4] R. Toledo-Moreo, M. A. Zamora-Izquierdo, B. Ubada-Minarro, and A. F. Gomez-Skarmeta, "High-integrity IMM-EKF-based road vehicle navigation with low-cost GPS/SBAS/INS," *IEEE Trans. Intell. Transp. Syst.*, vol. 8, no. 3, pp. 491–511, Sep. 2007.
- [5] R. Toledo-Moreo, D. Betaille, and F. Peyret, "Lane-level integrity provision for navigation and map matching with GNSS, dead reckoning, and enhanced maps," *IEEE Trans. Intell. Transp. Syst.*, vol. 11, no. 1, pp. 100–112, Mar. 2010.
- [6] K. Jo, K. Chu, and M. Sunwoo, "Interacting multiple-model filter-based sensor fusion of GPS with in-vehicle sensors for real-time vehicle positioning," *IEEE Trans. Intell. Transp. Syst.*, vol. 13, no. 1, pp. 329–343, Mar. 2012.
- [7] A. Ramanandan, A. Chen, and J. A. Farrell, "Inertial navigation aiding by stationary updates," *IEEE Trans. Intell. Transp. Syst.*, vol. 13, no. 1, pp. 235–248, Mar. 2012.
- [8] K. H. Senger and W. Kortum, "Investigations on state observers for the lateral dynamics of four-wheel steered vehicles," in *Proc. 11th IAVSD Symp., Suppl. Veh. Syst. Dyn.—Dynamics of Vehicles on Roads and on Tracks*, Kingston, ON, Canada, 1989, vol. 18, pp. 515–527.
- [9] L. R. Ray, "Nonlinear state and tire force estimation for advanced vehicle control," *IEEE Trans. Control Syst. Technol.*, vol. 3, no. 1, pp. 117–124, Mar. 1995.
- [10] J. Farrelly and P. Wellstead, "Estimation of vehicle lateral velocity," in *Proc. IEEE Int. Conf. Control Appl.*, Dearborn, MI, 1996, pp. 552–557.
- [11] C. S. Liu and H. Peng, "A state and parameter identification scheme for linearly parameterized systems," *ASME Trans.: J. Dyn. Syst., Meas. Control*, vol. 120, no. 4, pp. 524–528, Dec. 1998.
- [12] M. Kaminaga and G. Naito, "Vehicle body slip angle estimation using an adaptive observer," in *Proc. Int. Symp. Adv. Veh. Control*, 1998, pp. 207–212.
- [13] Y. Fukada, "Slip-angle estimation for vehicle stability control," *Veh. Syst. Dyn.*, vol. 32, no. 4/5, pp. 375–388, Nov. 1999.
- [14] H. E. Tseng, "A sliding model lateral velocity observer," in *Proc. 6th Int. Symp. AVEC*, Hiroshima, Japan, 2002, pp. 387–392.
- [15] A. Y. Ungoren, H. Peng, and H. E. Tseng, "A study on lateral speed estimation methods," *Int. J. Veh. Auton. Syst.*, vol. 2, no. 1/2, pp. 126–144, 2004.
- [16] H. Lee, "Reliability indexed sensor fusion and its application to vehicle velocity estimation," *Trans. ASME: J. Dyn. Syst. Meas. Control*, vol. 128, no. 2, pp. 236–243, 2006.
- [17] H. W. Son, "A study on design of a robust vehicle side-slip angle observer using an integration of kinematic and bicycle model," in *Proc. KSAE Annu. Conf.*, Daejeon, Korea, 2008.
- [18] S. H. You, J. O. Hahn, and H. C. Lee, "New adaptive approaches to real-time estimation of vehicle side-slip angle," *Control Eng. Pract.*, vol. 17, no. 12, pp. 1367–1379, Dec. 2009.
- [19] J. Kim, "Effect of vehicle model on the estimation of lateral vehicle dynamics," *Int. J. Autom. Technol.*, vol. 11, no. 3, pp. 331–337, 2010.
- [20] H. H. Kim and J. Ryu, "Side-slip angle estimation considering short-duration longitudinal velocity variation," *Int. J. Autom. Technol.*, vol. 12, no. 4, pp. 545–553, Aug. 2011.
- [21] A. Akhenak, M. Chadli, J. Ragot, and D. Maquin, "State estimation via multiple observers with unknown input: Application to the three-tank system," in *Proc. 5th IFAC SAFEPROCESS*, Washington, DC, 2003, pp. 245–251.
- [22] J. Oh and S. B. Choi, "Design of new multiple observers for vehicle velocity and attitude estimation," in *Proc. IASTED Int. Conf., Control Appl.*, Vancouver, BC, Canada, 2011, pp. 102–109.
- [23] P. A. Ioannou and J. Sun, *Robust Adaptive Control*. Englewood Cliffs, NJ: Prentice-Hall, 1964, p. 150.



**Jiwon J. Oh** received the B.S. and M.S. degrees in mechanical engineering from the Korea Advanced Institute of Science and Technology (KAIST), Daejeon, Korea.

He is currently a Researcher with the Automotive Control Laboratory, Department of Mechanical Engineering, KAIST. His research interests include vehicle state estimation and control.



**Seibum B. Choi** (M'09) received the B.S. degree in mechanical engineering from Seoul National University, Seoul, Korea, the M.S. degree in mechanical engineering from the Korea Advanced Institute of Science and Technology (KAIST), Daejeon, Korea, and the Ph.D. degree in controls from the University of California, Berkeley, in 1993.

From 1993 to 1997, he was with the Institute of Transportation Studies, University of California, Berkeley, where he was involved in the development of automated vehicle control systems. In 2006, he was with TRW, Warren, MI, where he was engaged in the development of advanced vehicle control systems. Since 2006, he has been with the faculty of the Department of Mechanical Engineering, KAIST. His research interests include fuel saving technology, vehicle dynamics and control, and active safety systems.